of the α-β plot for the reaction series under study reveals little variability in α within the series.

The correlation between β and γ, implied by the Hammond postulate, is of central interest. As one may conclude from the inspection of Figure 7, the presence of such correlation is confirmed for the series of chemical reactions in question, although there is a considerable scatter of points. In particular, the fact that one of the reactions ("HHHF") is both exothermic and possesses a late transition state cannot be overlooked.

Conclusions

The ability to quantify the parameters of empirical relationships is of a great importance. It not only allows for establishing quantitative correlations, but also aids in understanding their limits of validity. Once numerical values are available, the quality of correlations can be readily assessed with statistical methods.

The proposed indices make it possible to describe the characters of the transition states in a quantitative, yet concise, manner. They also provide the means for visualizing the structural relations between the reactants, the products, and the transition state. Series of similar reactions are expected to occupy distinct portions of the α-β graph, allowing for a general classification of chemical reactions.

The present definitions of exothermicity, structural proximity to reactants, and the isosynchronicity parameter use well-defined quantities that have transparent physical and chemical interpretations. The indices are readily calculated with the data available from the electronic structure calculations. As a side product, the optimized mutual orientations of the reactants, products, and transition states are obtained. A new concept of isosynchronicity, which describes the "straightforwardness" of the reaction path, is quantified with the aid of the parameter α.

The Hammond postulate, like any other empirical correlation, should be applied with caution. The relative proximities between the reactants, the products, and the transition state are only one of the several factors that determine the energetics of the forward and reverse reactions. In general, the larger the distance between the reaction center and the substituents that vary within the reaction series, the better correlation between β and γ can be expected.

Acknowledgment. This work was partially supported by the National Science Foundation under the Contract CHE-9015566, the Camille and Henry Dreyfus Foundation New Faculty Award Program, and the Florida State University through time granted on its Cray Y-MP digital computer.

Covalent vs Ionic Bonding in Hexasubstituted "Push-Pull" Ethanes

Stacey T. Mixon and Jerzy Cioslowski*

Contribution from the Department of Chemistry and Supercomputer Computations Research Institute, Florida State University, Tallahassee, Florida 32306-3006.
Received December 20, 1990

Abstract: HF/6-31G* electronic structure calculations reveal the presence of a covalent central C–C bond in the $C(NH_2)_3CF_3$ molecule, whereas the $C(NH_2)_3C(NO_2)_3$ species is found to be best described as an ionic pair. The $C(NH_2)_3C(CN)_3$ molecule exists as either a covalent or an ionic isomer. These observations are derived from the optimized geometries of various rotamers of the "push-pull" hexasubstituted ethanes $C(NH_2)_3CX_3$, where X = F, CN, or NO_2, which are characterized as either minima or transition states according to the calculated vibrational frequencies. Additional confirmation of the presence of either covalent or ionic bonding is provided by the calculated GAPT charges and charge transfers, and by Bader atomic charges. The molecular graphs of the push-pull ethanes, as defined within the topological theory of atoms in molecules, exhibit very complicated patterns of bonding rich in weak bonds and unexpected ring and cage points.

Introduction

The effects of substituents on chemical properties of molecules are well known and understood by organic chemists. Phenomena such as the increase in acidity upon substitution by fluorine atoms, or the weakening of basicity upon phenyl substitution in amines, are textbook examples. In some molecules, the substituent effects are quite dramatic. For example, tricyanomethane and trinitromethane are strong acids in water, whereas methane itself manifests acidity under only very extreme conditions. Similarly, the triaminomethyl cation is one of the most stable carbocations known in organic chemistry.[1] Even such strong effects, however, do not usually result in a total alteration of the electronic structure.

The ethane molecule possesses a covalent central bond that requires about 88 kcal/mol to be cleaved homolytically. One may inquire how the C–C bonding in ethane could be influenced by the presence of several substituents on the carbon atoms. In particular, an arrangement where the electron-withdrawing substituents, X, are attached to one atom and the electron-donating substituents, Y, are attached to the other atom is of great interest. In an extreme situation, the resulting polarization of the C–C bond might bring about an ionic dissociation of the molecule, yielding an ionic pair. One could also contemplate the possibility of the existence of two isomers, the covalent one best described as CY_3CX_3 and the ionic one best formulated as CY_3^+ CX_3^-.

Let us review the possible factors influencing the relative stabilities of the covalent and ionic isomers of this kind. The covalent molecule is stabilized by the presence of a strong single C–C bond, which must be at least partially dissociated in the ionic isomer. On the other hand, the ionic species may lower its energy through either inductive or mesomeric stabilization of the CX_3^- and CY_3^+ ions. Moreover, if the substituents X and Y are bulky, the steric destabilization is relieved in the ionic form due to the fact that the distance between X and Y is expected to be much larger in the ionic species than in the covalent one. Finally, should either CX_3^- or CY_3^+ be stabilized through Y resonance,[1,2] the preferable sp^2 hybridization of the central carbon atom is feasible only in

* To whom correspondence should be addressed.

(1) Gund, P. *J. Chem. Educ.* **1972**, *49*, 100.
(2) Jordan, M. J.; Gready, J. E. *J. Comput. Chem.* **1989**, *10*, 186 and the references cited therein.

0002-7863/91/1513-6760$02.50/0

the ionic isomer. In summary, when the three aforementioned effects overcome the energy of (partially) cleaving the covalent C–C bond, then one may expect the ionic isomer to be more stable than the covalent one.

Although known to be strongly electron withdrawing, none of the fluoro, cyano, and nitro substituents is capable of causing the C–H bond to dissociate in the trisubstituted methanes. In fact, the calculated proton affinities of the CX_3^- (X = F, CN, or NO_2) molecules are well above 300 kcal/mol.[3,4] One may, however, try an approach of concerted "pushing" and "pulling" the electrons by putting three of the above substituents on one of the carbon atoms of the ethane molecule, while attaching three electron-donating amino groups to the other. The resulting "push–pull" hexasubstituted ethanes are the object of our theoretical study.

There are several reports on the ionic dissociation of C–C bonds published in the chemical literature. The heterolytic cleavage in these systems is usually due to the influence of a polar solvent. Examples of such behavior include cyclopropanes[5] and derivatives of malononitrile.[6] Extensive experimental studies to determine and correlate bond heterolysis and homolysis energies in solution have been recently undertaken by Arnett et al.[7] Okamoto and co-workers reported synthesis of an unsubstituted hydrocarbon in which heterolytic C–C cleavage is induced by crystallization.[8] On the other hand, the experimental evidence for the existence of push–pull ethanes of the type CY_3CX_3 is quite scarce. Our extensive literature searches produced no references to the $C(NH_2)_3CF_3$ system. Formation of the corresponding cyano derivative $C(NH_2)_3C(CN)_3$ has been previously reported.[9] We have also recently published a preliminary account on the electronic structure of this molecule.[10] The nitro derivative $C(NH_2)_3C(NO_2)_3$ has been described in conjunction with its possible usage as a high explosive.[11] A report on the same compound has appeared recently in the chemical literature;[12] however, the reported melting point is in disagreement with that given in ref 11. The same paper[12] reports results of low-level (HF/3-21G) ab initio calculations on the cyano and nitro derivatives.

Computational Techniques

The molecular geometries were optimized at the HF/6-31G* level[13] by using the GAUSSIAN 88 suite of codes,[14] running on the VAXstation 3540 and the Cray Y-MP 4/32 supercomputer. All vibrational frequencies were calculated at the same level of theory.

The electron density was analyzed within the framework of the topological theory of atoms in molecules,[15–17] which defines the major elements of molecular structure, such as bonds, rings, and cages, in terms of the critical points in the electron density, $\rho(\vec{r})$. In this theory, an atom consists of a nucleus and its associated atomic basin. An atomic basin is the region traced out by the paths of steepest descent in the electron density that originate from the nucleus in question. Some pairs of atoms are connected by gradient paths that originate at the nuclei and terminate at a common point where $\nabla\rho = 0$. This critical point is a minimum point along a path of maximum electron density and is called a bond point. The associated path is called a bond path. By indicating the major interactions (bonds) between atoms, the set of all bond paths defines molecular structure in a topological sense. To characterize atomic interactions, one can calculate the values of $\rho(\vec{r})$ and $\nabla^2\rho(\vec{r})$ at the bond critical points; these values are denoted ρ_{crit} and $\nabla^2\rho_{crit}$, respectively. Bond orders can be correlated with ρ_{crit},[15] whereas the sign of $\nabla^2\rho_{crit}$ can serve as an indicator of bond type.[16] Positive values of $\nabla^2\rho_{crit}$ are characteristic of closed shell interactions, such as ionic, van der Waals, and hydrogen bonding. Negative values indicate shared interactions, as in covalent bonds. The topological theory also provides a method of calculating atomic properties, such as atomic charges, by integrating appropriate products of wave functions and operators over atomic basis.[17] The topological properties of atoms and bonds that we report here were calculated with the EXTREM and PROAIM programs of Bader et al.[17]

The recently proposed GAPT partitioning method[18] was also used to calculate effective atomic charges. The GAPT atomic charges, which are equal to one-third of the traces of the tensors of derivatives of the molecular dipole moments with respect to the nuclear Cartesian coordinates, have been repeatedly proven to provide a good representation of the electron distributions in many diverse systems.[19]

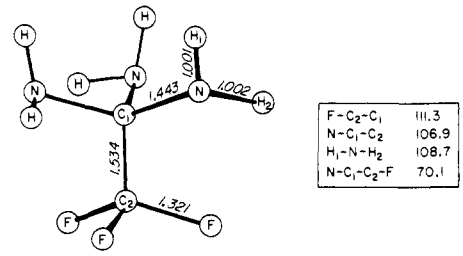

Figure 1. HF/6-31G* optimized geometry of the C_3 minimum of the $C(NH_2)_3CF_3$ molecule (**1**).

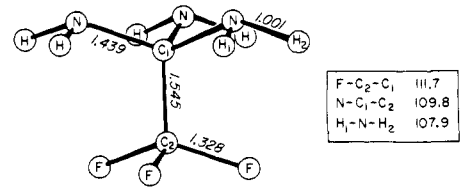

Figure 2. HF/6-31G* optimized geometry of the staggered transition state of the $C(NH_2)_3CF_3$ molecule (**2**).

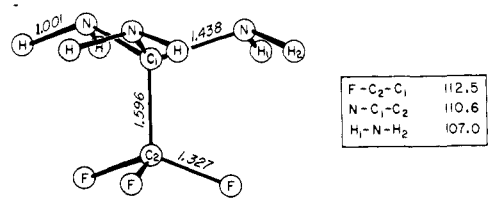

Figure 3. HF/6-31G* optimized geometry of the eclipsed transition state of the $C(NH_2)_3CF_3$ molecule (**3**).

Results and Discussion

The stabilization energies (E_{stab}) for all species studied are listed in Table I, along with the corresponding numbers of imaginary eigenvalues of the energy Hessian (N), the calculated Hartree–Fock total energies (E_{HF}) and dipole moments (μ_{HF}), and the

(3) Edgecombe, K. E.; Boyd, R. J. *Can. J. Chem.* **1983**, *61*, 45. Edgecombe, K. E.; Boyd, R. J. *Can. J. Chem.* **1984**, *62*, 2887.
(4) Cioslowski, J.; Mixon, S. T.; Fleischmann, E. D. *J. Am. Chem. Soc.* **1991**, *113*, 4751.
(5) Yankee, E. W.; Badea, F. D.; Howe, N. E.; Cram, D. J. *J. Am. Chem. Soc.* **1973**, *95*, 4210.
(6) Mitsuhashi, T.; Hirota, H. *J. Chem. Soc., Chem. Commun.* **1990**, 324.
(7) Arnett, E. M.; Amarnath, K.; Harvey, N. G.; Cheng, J. P. *J. Am. Chem. Soc.* **1990**, *112*, 344.
(8) Okamoto, K.; Kitagawa, T.; Takeuchi, K.; Komatsu, K.; Miyabo, A. *J. Chem. Soc., Chem. Commun.* **1988**, 923.
(9) Pentin, Yu. A.; Makhon'kov, D. I.; D'yakova, L. Ya.; Baburina, I. I.; Zefirov, N. S. *Zh. Obshch. Khim.* **1978**, *8*, 1850.
(10) Cioslowski, J.; Mixon, S. T. *Chem. Phys. Lett.* **1990**, *170*, 297.
(11) Fedoroff, B. T.; Sheffield, O. E. *Encyclopedia of Explosives and Related Items*; Picatinny Arsenal: Dover, NJ, 1974; p G151 and the references cited therein.
(12) Krishnan, A. M.; Sjoberg, P.; Politzer, P.; Boyer, H. J. *J. Chem. Soc., Perkin Trans. 2* **1989**, 1237.
(13) Hariharan, P. C.; Pople, J. A. *Theor. Chim. Acta* **1973**, *28*, 213.
(14) GAUSSIAN 88: Frisch, M. J.; Head-Gordon, M.; Schlegel, H. B.; Raghavachari, K.; Binkley, J. S.; Gonzalez, C.; Defrees, D. J.; Fox, D. J.; Whiteside, R. A.; Seeger, R.; Melius, C. F.; Baker, J.; Martin, R. L.; Kahn, L. R.; Stewart, J. J. P.; Fluder, E. M.; Topiol, S.; Pople, J. A. Gaussian, Inc.: Pittsburgh, PA.
(15) Bader, R. F. W.; Tal, Y.; Anderson, S. G.; Nguyen-Dang, T. T. *Isr. J. Chem.* **1980**, *19*, 8. Bader, R. F. W.; Tang, T. H.; Tal, Y.; Biegler-König, F. W. *J. Am. Chem. Soc.* **1982**, *104*, 940, 946. Bader, R. F. W.; Nguyen-Dang, T. T.; Tal, Y. *Rep. Prog. Phys.* **1981**, *44*, 893. Bader, R. F. W.; Nguyen-Dang, T. T. *Adv. Quantum Chem.* **1981**, *14*, 63. Bader, R. F. W.; Slee, T. S.; Cremer, D.; Kraka, E. *J. Am. Chem. Soc.* **1983**, *105*, 5061.
(16) Bader, R. F. W.; Essen, H. *J. Chem. Phys.* **1984**, *80*, 1943.
(17) Biegler-König, F. W.; Bader, R. F. W.; Tang, T. H. *J. Comput. Chem.* **1982**, *3*, 317.
(18) Cioslowski, J. *J. Am. Chem. Soc.* **1989**, *111*, 8333.
(19) Cioslowski, J.; Hay, P. J. *J. Am. Chem. Soc.* **1990**, *112*, 1707. Cioslowski, J.; Hay, P. J.; Ritchie, J. P. *J. Phys. Chem.* **1990**, *94*, 148. Cioslowski, J.; Hamilton, T.; Scuseria, G.; Hess, B. A., Jr.; Hu, J.; Schaad, L. J.; Dupuis, M. *J. Am. Chem. Soc.* **1990**, *112*, 4183. Cioslowski, J. *J. Am. Chem. Soc.* **1990**, *112*, 6536. Cioslowski, J.; Fleischmann, E. D. *J. Chem. Phys.* **1991**, *94*, 3730.

Table I. Calculated HF/6-31G* Total Energies, Stabilization Energies, Numbers of Imaginary Frequencies, Dipole Moments and GAPT Charge Transfers in $C(NH_2)_3CX_3$

X	structure	N^a	E_{HF} (au)	$E_{stab}{}^b$ (kcal/mol)	μ_{HF} (D)	ΔQ_{GAPT}
F	C_3 minimum	0	-540.893 554	159.66 (154.25)	4.5229	0.0929
	staggered TS	1	-540.884 484	153.97	1.8860	0.2765
	eclipsed TS	2	-540.870 549	145.23	1.8336	0.3066
CN	C_3 covalent minimum	0	-519.464 482	60.24 (57.43)	7.5357	0.2723
	C_3 ionic minimum	0	-519.499 018	81.92 (79.83)	7.5282	0.9325
	staggered TS	1	-519.454 824	54.18	1.4478	0.7004
	eclipsed TS	1	-519.489 744	76.10	9.5592	0.9602
NO_2	C_3 "minimum"	2	-854.682 352	83.64 (81.34)	8.3694	0.9710
	staggered TS	4	-854.656 764	67.59	9.0190	0.9746
	eclipsed TS	4	-854.656 683	67.54	9.2726	0.9825

[a] Number of imaginary frequencies. [b] Values corrected for the zero-point energy are given in parentheses.

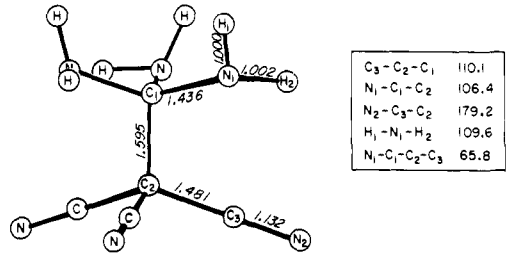

Figure 4. HF/6-31G* optimized geometry of the covalent C_3 minimum of the $C(NH_2)_3C(CN)_3$ molecule (**4**).

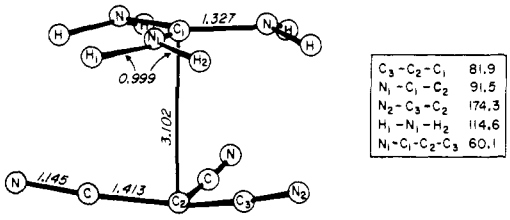

Figure 5. HF/6-31G* optimized geometry of the ionic C_3 minimum of the $C(NH_2)_3C(CN)_3$ molecule (**5**).

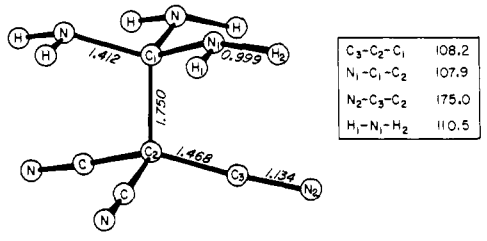

Figure 6. HF/6-31G* optimized geometry of the staggered transition state of the $C(NH_2)_3C(CN)_3$ molecule (**6**).

GAPT charge transfers (ΔQ_{GAPT}). The stabilization energies are calculated as

$$E_{stab}(CY_3CX_3) = E_{HF}(CY_3^+) + E_{HF}(CX_3^-) - E_{HF}(CY_3CX_3) \qquad Y = NH_2 \quad (1)$$

We also report in Table I the values of the stabilization energy incorporating the zero-point energy for the minimum-energy structures. The process described by eq 1 can formally be regarded as a heterolytic bond cleavage. For comparison, the homolytic bond dissociation energy of ethane is about 88 kcal/mol. The $C(NH_2)_3CF_3$ molecule (**1**) has the highest stabilization energy, which is greatly reduced in the corresponding covalent minimum of the $C(NH_2)_3C(CN)_3$ molecule (**4**). It is interesting to note the higher stability of the C_3 "minimum" structure of $C(NH_2)_3C(NO_2)_3$ (**8**) than that of the ionic minimum of $C(NH_2)_3C(CN)_3$ (**5**). As will be shown below, this isomer has hydrogen bonding between the amino and nitro groups that contributes some extra stability to it.

The GAPT charge transfer, which is equal to the sum of all GAPT charges in the guanidinium moiety, clearly indicates which structures are ionic (with almost complete transfer of one electron

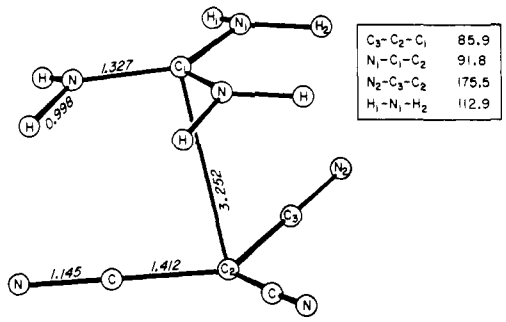

Figure 7. HF/6-31G* optimized geometry of the eclipsed transition state of the $C(NH_2)_3C(CN)_3$ molecule (**7**).

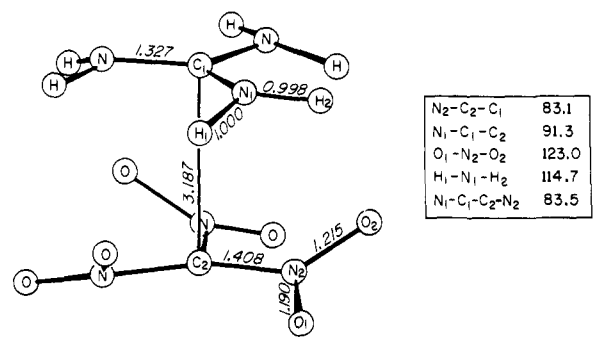

Figure 8. HF/6-31G* optimized geometry of the C_3 minimum of the $C(NH_2)_3C(NO_2)_3$ molecule (**8**).

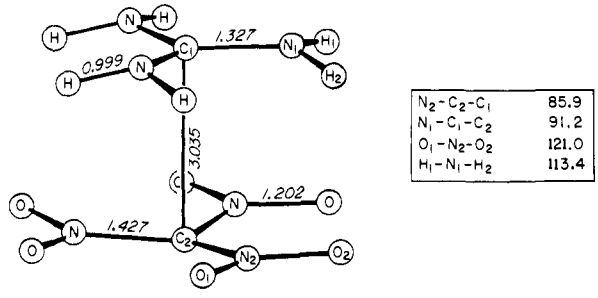

Figure 9. HF/6-31G* optimized geometry of the staggered transition state of the $C(NH_2)_3C(NO_2)_3$ molecule (**9**).

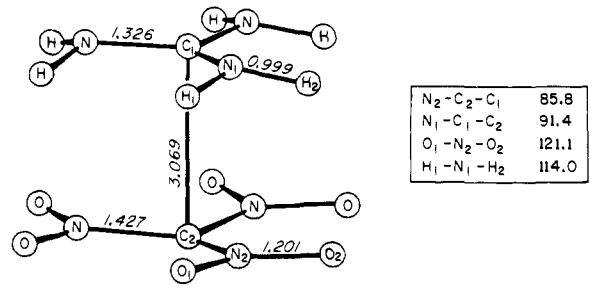

Figure 10. HF/6-31G* optimized geometry of the eclipsed transition state of the $C(NH_2)_3C(NO_2)_3$ molecule (**10**).

Table II. Calculated Topological Properties of the Bond Points in $C(NH_2)_3CF_3$[a]

bond	r_1 (au)	r_2 (au)	ρ_{crit} (au)	$\nabla^2\rho_{crit}$ (au)	ϵ
		C_3 Minimum (**1**)			
C_1–C_2	1.3327	1.5669	0.2844	−0.8938	0.0000
C_2–F	0.7948	1.7018	0.2793	0.2996	0.2047
C_1–N	1.0476	1.6804	0.2946	−1.0828	0.0676
N–H_1	1.4147	0.4777	0.3435	−1.7364	0.0467
N–H_2	1.4282	0.4644	0.3440	−1.7604	0.0414
		Staggered TS (**2**)			
C_1–C_2	1.2817	1.6377	0.2757	−0.8438	0.0000
C_2–F	0.7974	1.7113	0.2725	0.3267	0.2559
C_1–N	1.0647	1.6552	0.2986	−1.1047	0.0627
N–H_1	1.4184	0.4736	0.3445	−1.7512	0.0451
N–H_2	1.4184	0.4736	0.3445	−1.7512	0.0451
		Eclipsed TS (**3**)			
C_1–C_2	1.3313	1.6842	0.2484	−0.6865	0.0000
C_2–F	0.7970	1.7104	0.2734	0.3252	0.2366
C_1–N	1.0727	1.6466	0.2998	−1.1051	0.0507
N–H_1	1.4160	0.4762	0.3451	−1.7536	0.0439
N–H_2	1.4160	0.4762	0.3451	−1.7536	0.0439

[a] The distance between the critical point and the first (second) atom listed is denoted by r_1 (r_2). ϵ stands for the bond ellipticity.[20]

from the guanidinium to the haloformide fragment) and which ones are covalent (with sharing of electrons between the fragments). One should note that the total dipole moment is not a good indicator of covalency or ionicity for these structures because of the large contributions from the polar groups attached to each of the carbon atoms. A remarkable result of this study is the existence of two stable isomers of 1,1,1-triamino-2,2,2-tricyanoethane: one covalent (**4**), and the other ionic (**5**).

The HF/6-31G* optimized geometries of all molecules studied are displayed in Figures 1–10. One should note the large variations in the central C–C bond lengths. Also, the "inverted umbrella" (or "anti-sp^3") arrangements of the bonds in the $C(CN)_3^-$ and $C(NO_2)_3^-$ moieties of the ionic conformers, characteristic of delocalized ionic bonding,[10] are worth mentioning. The patterns of bond lengths in the CX_3 portions of the covalent systems resemble those in the CHX_3 molecules, whereas the patterns of the ionic systems exhibit similarities to those in the CX_3^- ions.

A few comments about the imaginary frequencies of the transition states are in order. In the $C(NH_2)_3C(CN)_3$ species (**6** and **7**), these frequencies correspond to rotation of the amino groups. The same is true in the $C(NH_2)_3CF_3$ structures (**2** and **3**), but the eclipsed transition state has an extra imaginary frequency corresponding to amino group rotation mixed with some rotation about the carbon–carbon central bond. The imaginary frequencies in the transition states of $C(NH_2)_3C(NO_2)_3$ (**9** and **10**) correspond to combinations of amino and nitro group rotations. The C_3 conformer (**8**) that we denote as minimum has two small imaginary frequencies due to rotation of the nitro groups. These frequencies are equal to about 33i cm^{-1}, while the imaginary frequencies in the transition states are of the order of 100i–200i cm^{-1}. Due to the complexity of the potential energy surface, it is extremely difficult to locate the true minimum in this case, and because of the expense of these calculations, we did not attempt further optimization. Because the two imaginary frequencies are so small, we feel confident that the structure displayed in Figure 8 is not far from the true minimum geometry and that its total energy reported in Table I is very close to the true energy.

The results of the topological analysis of the electron densities of the molecules under study are given in Tables II–IV for the fluoro-, cyano-, and nitro-substituted ethanes, respectively. Note that, in the guanidinium portions of each structure, the properties of the N–H bonds are fairly constant. The same is true of the distances from the amino nitrogens to the C–N bond critical points, but the distances from the carbon atoms to these critical points are much larger in the covalent isomers than in the ionic ones. Just the opposite trend is observed in the values of ρ_{crit} and $\nabla^2\rho_{crit}$ at these bond points; the values of these quantities are larger in

Table III. Calculated Topological Properties of the Bond Points in $C(NH_2)_3C(CN)_3$[a]

bond	r_1 (au)	r_2 (au)	ρ_{crit} (au)	$\nabla^2\rho_{crit}$ (au)	ϵ
		C_3 Covalent Minimum (**4**)			
C_1–C_2	1.3808	1.6327	0.2339	−0.6052	0.0000
C_2–C_3	1.2837	1.5144	0.2717	−0.8113	0.0396
C_3–N_2	0.7251	1.4149	0.4900	0.9028	0.0046
C_1–N_1	1.0580	1.6564	0.3012	−1.1240	0.0704
N_1–H_1	1.4231	0.4672	0.3430	−1.7469	0.0474
N_1–H_2	1.4334	0.4596	0.3426	−1.7559	0.0425
		C_3 Ionic Minimum (**5**)			
C_1–C_2 (*)	2.6996	3.1631	0.0093	0.0321	0.0000
C_2–C_3	1.1120	1.5581	0.2921	−0.9013	0.4154
C_3–N_2	0.7344	1.4295	0.4829	0.5034	0.0898
C_1–N_1	0.8528	1.6554	0.3654	−1.2656	0.0733
N_1–H_1	1.4597	0.4281	0.3387	−1.7715	0.0371
N_1–H_2	1.4596	0.4281	0.3388	−1.7718	0.0371
		Staggered TS (**6**)			
C_1–C_2	1.4492	1.8584	0.1644	−0.2669	0.0000
C_2–C_3	1.2447	1.5298	0.2742	−0.8236	0.0917
C_3–N_2	0.7264	1.4170	0.4896	0.8353	0.0176
C_1–N_1	1.0403	1.6301	0.3164	−1.2413	0.0488
N_1–H_1	1.4277	0.4606	0.3439	−1.7627	0.0458
N_1–H_2	1.4277	0.4606	0.3439	−1.7627	0.0458
		Eclipsed TS (**7**)			
C_1–C_2 (*)	2.8150	3.3305	0.0074	0.0235	0.0000
C_2–C_3	1.1175	1.5504	0.2927	−0.9038	0.4106
C_3–N_2	0.7343	1.4290	0.4829	0.5109	0.0866
C_1–N_1	0.8519	1.6557	0.3651	−1.2568	0.0750
N_1–H_1	1.4550	0.4300	0.3403	−1.7808	0.0371
N_1–H_2	1.4550	0.4300	0.3403	−1.7808	0.0371
N_1–N_2 (*)	3.1137	3.0109	0.0080	0.0254	0.7955

[a] The distance between the critical point and the first (second) atom listed is denoted by r_1 (r_2). ϵ stands for the bond ellipticity.[20] The weak bonds are marked by (*).

Table IV. Calculated Topological Properties of the Bond Points in $C(NH_2)_3C(NO_2)_3$[a]

bond	r_1 (au)	r_2 (au)	ρ_{crit} (au)	$\nabla^2\rho_{crit}$ (au)	ϵ
		C_3 "Minimum" (**8**)			
C_1–C_2 (*)	2.8114	3.2107	0.0073	0.0264	0.0000
C_2–N_2	0.8485	1.8119	0.2969	−0.3768	1.4150
N_2–O_1	1.0917	1.1570	0.5535	−1.3950	0.1419
N_2–O_2	1.1245	1.1719	0.5216	−1.2326	0.1205
C_1–N_1	0.8521	1.6552	0.3656	−1.2601	0.0815
N_1–H_1	1.4554	0.4303	0.3405	−1.7807	0.0371
N_1–H_2	1.4668	0.4226	0.3370	−1.7661	0.0365
N_1–O_2 (*)	2.8847	3.6363	0.0087	0.0321	0.5449
O_1–O_2 (*)	2.5523	2.5373	0.0164	0.0687	0.4150
O_2–H_2 (*)	1.8243	2.7204	0.0114	0.0458	0.2756
		Staggered TS (**9**)			
C_1–C_2 (*)	2.6668	3.0684	0.0104	0.0354	0.0000
C_2–N_2	0.8784	1.8183	0.2898	−0.5772	1.2658
N_2–O_1	1.1143	1.1567	0.5378	−1.2733	0.1182
N_2–O_2	1.1143	1.1567	0.5378	−1.2733	0.1182
C_1–N_1	0.8527	1.6550	0.3649	−1.2574	0.0795
N_1–H_1	1.4595	0.4275	0.3389	−1.7739	0.0369
N_1–H_2	1.4595	0.4275	0.3389	−1.7739	0.0369
N_1–O_1 (*)	2.9514	3.0988	0.0071	0.0280	0.7295
N_1–O_2 (*)	2.9514	3.0988	0.0071	0.0280	0.7295
O_1–O_2 (*)	2.3044	2.3044	0.0272	0.1229	0.0943
		Eclipsed TS (**10**)			
C_1–C_2 (*)	2.6934	3.1064	0.0097	0.0325	0.0000
C_2–N_2	0.8781	1.8180	0.2901	−0.5771	1.2643
N_2–O_1	1.1138	1.1566	0.5382	−1.2765	0.1184
N_2–O_2	1.1138	1.1566	0.5382	−1.2765	0.1184
C_1–N_1	0.8517	1.6550	0.3650	−1.2521	0.0795
N_1–H_1	1.4603	0.4271	0.3385	−1.7711	0.0372
N_1–H_2	1.4603	0.4271	0.3385	−1.7711	0.0372
N_1–N_2 (*)	2.9618	2.7082	0.0088	0.0345	0.0196
O_1–O_2 (*)	2.3016	2.3016	0.0274	0.1240	0.0965

[a] The distance between the critical point and the first (second) atom listed is denoted by r_1 (r_2). ϵ stands for the bond ellipticity.[20] The weak bonds are marked by (*).

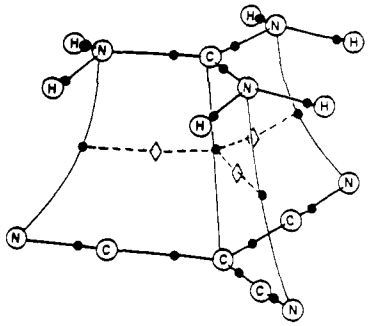

Figure 11. Molecular graph of the eclipsed transition state of the $C(NH_2)_3C(CN)_3$ molecule (**7**). Bond points are denoted by heavy dots, ring points by diamonds, and cage points by stars.

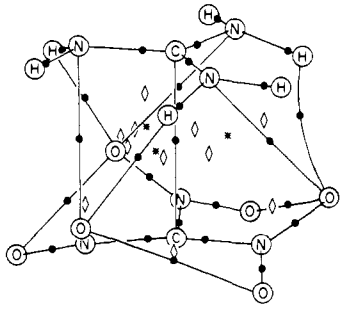

Figure 12. Molecular graph of the C_3 minimum of the $C(NH_2)_3C(NO_2)_3$ molecule (**8**). Bond points are denoted by heavy dots, ring points by diamonds, and cage points by stars.

the ionic series than in the covalent series. This effect, whose origin can be traced to the variations in the C_1–N_1 bond lengths, is more pronounced in the Laplacian, as would be expected because the Laplacian is a second-derivative quantity and is thus more sensitive. The value of $\nabla^2\rho_{crit}$ at the C_1–N_1 bond critical point in the staggered rotamer of $C(NH_2)_3C(CN)_3$ (**6**) is anomalous, resembling more the values for the ionic compounds. This is the result of steric hindrance brought about by the presence of bulky amino and cyano groups in this structure. Although still covalent, the carbon–carbon bond in this molecule is quite stretched (the carbon–carbon bond distance is 1.75 Å; see Figure 6), which precipitates the onset of ionic dissociation. This also results in the large value of the GAPT charge transfer for this rotamer.

We are gratified to note that the signs of $\nabla^2\rho_{crit}$ at the critical points between the central carbon atoms in all systems studied indicate the same bond type as we predict on the basis of the GAPT charge transfer. The calculated magnitudes of ρ_{crit} fall into two categories that parallel the division by the carbon–carbon bond type. As expected from the differences in bond lengths, ρ_{crit} is much smaller in the ionic structures than in the covalent ones. As indicated earlier, the value of the electron density can give an estimate of the bond order.[15] The bond orders for the ionic bonds are equal to about 0.2.

The molecular graph[15] of the eclipsed rotamer of $C(NH_2)_3C(CN)_3$ shown in Figure 11, which was previously reported,[10] deserves special comment. In addition to bond points between atoms that one would expect to be bonded on the basis of "chemical intuition", the electron density of this system reveals the existence of three ring points and three additional bond points. These extra bond points correspond to high-ellipticity[20] bonds connecting the nitrogen atoms of the amino and cyano groups. Like the central carbon–carbon bond, these additional bonds arise from delocalized ionic interactions between the triaminocarbenium and tricyanomethanide fragments of the molecule.

The molecular graphs of all the $C(NH_2)_3C(NO_2)_3$ conformers studied also feature unusual bonding (Figures 12–14). All three

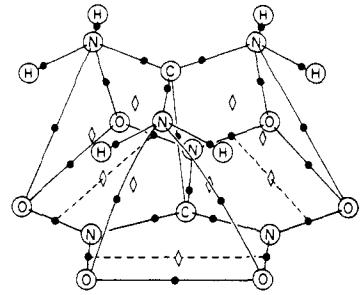

Figure 13. Molecular graph of the staggered transition state of the $C(NH_2)_3C(NO_2)_3$ molecule (**9**). Bond points are denoted by heavy dots, ring points by diamonds, and cage points by stars.

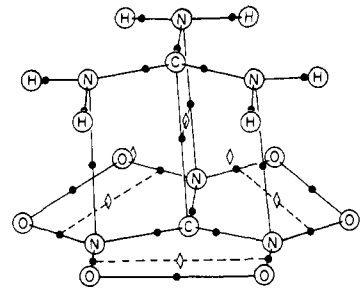

Figure 14. Molecular graph of the eclipsed transition state of the $C(NH_2)_3C(NO_2)_3$ molecule (**10**). Bond points are denoted by heavy dots, ring points by diamonds, and cage points by stars.

Table V. Calculated Bader and GAPT Atomic Charges in $C(NH_2)_3CF_3$

	structure					
	C_3 minimum (**1**)		staggered TS (**2**)		eclipsed TS (**3**)	
atom	Q_{Bader}	Q_{GAPT}	Q_{Bader}	Q_{GAPT}	Q_{Bader}	Q_{GAPT}
C_1	1.3752	0.8787	1.3924	0.8858	1.4125	0.9216
C_2	2.0427	1.6355	1.9377	1.4794	1.8458	1.4448
N	−1.2034	−0.6068	−1.1480	−0.5587	−1.1242	−0.5469
H_1	0.3751	0.1554	0.3880	0.1778	0.3811	0.1709
H_2	0.4083	0.1896	0.3880	0.1778	0.3811	0.1709
F	−0.7477	−0.5761	−0.7543	−0.5853	−0.7567	−0.5838

systems show the weak oxygen–oxygen bonds that were recently uncovered in the trinitromethanide ion.[4,21] However, each system also exhibits its own characteristic pattern of bonding. In the staggered conformer (**9**), every amino nitrogen is bonded to an oxygen atom from each of two adjacent nitro groups. One would expect to find a ring point in each of the triangular regions bounded by two nitrogen–oxygen weak bonds and an oxygen–oxygen weak bond (see Figures 9 and 13). Yet, there are no ring points in these spaces, nor are there any cage points in this system. This observation can be elucidated by considering the analogous example of a three-membered ring. In that case, each pair of atoms is connected by a bond point, and there is a ring point in the interior of the ring. As one of the bond angles is increased, the bond opposite the vertex of the angle stretches, and the bond point approaches the ring point. Eventually, they coalesce into a degenerate critical point which is a catastrophe point.[22] If the bond angle is increased infinitesimally beyond this point, the two points annihilate each other and the bond is broken. In the present case, a similar effect occurs in three dimensions. The ring and cage points have been annihilated, leaving a "tunnel" with walls composed of atomic surfaces that pierces the plane of the ring. The resulting molecular graph satisfies the Poincare–Hopf relationship:[23]

$$n - b + r - c = 1 \qquad (2)$$

(20) The bond ellipticity, ϵ, is defined as $\epsilon = (\lambda_1/\lambda_2) - 1$, where λ_1 and λ_2 are the values of the negative curvatures of the electron density at the bond critical point along the axes perpendicular to the bond path.[16]

(21) Cioslowski, J.; Mixon, S. T.; Edwards, W. D. *J. Am. Chem. Soc.* **1991**, *113*, 1083.

(22) Bader, R. F. W. *Acc. Chem. Res.* **1985**, *18*, 9.

Table VI. Calculated Bader and GAPT Atomic Charges in $C(NH_2)_3C(CN)_3$

	structure							
	covalent minimum (**4**)		ionic minimum (**5**)		staggered TS (**6**)		eclipsed TS (**7**)	
atom	Q_{Bader}	Q_{GAPT}	Q_{Bader}	Q_{GAPT}	Q_{Bader}	Q_{GAPT}	Q_{Bader}	Q_{GAPT}
C_1	1.4379	1.1009	*a*	1.4829	1.5611	1.4982	*a*	1.4942
C_2	0.3965	0.4511	*a*	−0.6148	0.3497	−0.0275	0.3916	−0.6712
N_1	−1.2157	−0.6446	*a*	−0.8046	−1.2013	−0.7007	−1.4327	−0.7860
H_1	0.4008	0.1705	0.4999	0.3107	0.4180	0.2174	0.4958	0.3040
H_2	0.4199	0.1979	0.4997	0.3105	0.4180	0.2174	0.4958	0.3040
C_3	1.2253	0.0449	0.9592	0.5523	1.1915	0.0864	1.1456	0.5593
N_2	−1.4436	−0.2860	*a*	−0.6582	−1.4637	−0.3107	*a*	−0.6556

[a] The atomic charge could not be evaluated within the necessary accuracy due to the complicated shape of the respective atomic boundary.

Table VII. Calculated GAPT Atomic Charges in $C(NH_2)_3C(NO_2)_3$

	structure		
atom	C_3 minimum (**8**)	staggered TS (**9**)	eclipsed TS (**10**)
C_1	1.4497	1.4327	1.4804
C_2	−0.8300	−0.8019	−0.8002
N_1	−0.8028	−0.7801	−0.7972
H_1	0.3083	0.3137	0.3156
H_2	0.3349	0.3137	0.3156
N_2	1.5690	1.4906	1.4939
O_1	−0.7602	−0.7741	−0.7774
O_2	−0.8557	−0.7741	−0.7774

where *n* is the number of attractors (nuclei), *b* is the number of bonds, *r* is the number of rings, and *c* is the number of cages.

In the eclipsed conformer (**10**), there are three unusual nitrogen–nitrogen bonds between the amino and cyano groups, reminiscent of the bonding situation in the eclipsed conformer of $C(NH_2)_3C(CN)_3$. Also, a ring point is found in each of the three planes containing the N_1–C_1, C_1–C_2, C_2–N_2, and N_1–N_2 bonds (see Figures 10 and 14). The C_3 minimum structure of $C(NH_2)_3C(NO_2)_3$ (**8**) shows the most complicated pattern of bonding yet. In addition to the oxygen–oxygen bond paths referred to above, the oxygen atom nearer the guanidinium fragment in each nitro group is connected by bond paths to the nitrogen in the nearest amino group and to the nearer hydrogen in the amino group adjacent to that group (see Figures 8 and 12). Unlike the staggered case, here we find three cage points symmetrically disposed about the central carbon–carbon bond.

The HF/6-31G* GAPT and Bader atomic charges are given for the fluoro- and cyano-substituted species in Tables V and VI, respectively. The HF/6-31G* GAPT charges are given for the nitro-substituted species in Table VII. The atomic basins in the latter systems have extremely complex shapes, which prevent accurate determination of Bader charges. For comparison purposes, the HF/6-31G* GAPT and Bader atomic charges are given for trifluoro-, tricyano-, and trinitromethane, and their conjugate bases, in Table VIII.[4] Inspection of the tables reveals a number of trends. First, the magnitudes of both Bader and GAPT hydrogen charges provide a clear-cut classification of the structures under study into two groups: the covalent ones (**1**, **2**, **3**, **4**, and **6**) and the ionic ones (**5**, **7**, **8**, **9**, and **10**). In each series, the charges are fairly constant. The GAPT charges on hydrogens in ionic structures are about double the GAPT charges on hydrogens in covalent structures. The Bader hydrogen charges do not have such a dramatic difference, but the dichotomy is still evident.

Comparison of the atomic charges in the electron-withdrawing moiety of each structure with the same moiety in the trisubstituted methane or its anion aids in the classification of each structure as ionic or covalent. In all conformers of the $C(NH_3)CF_3$ molecule (**1**–**3**), the charge on the C_2 atom is large and positive for both definitions of atomic charge; this can be attributed to a strong electron-withdrawing effect of the fluorine substituent. The carbon and fluorine charges resemble the charges on carbon and fluorine in the CHF_3 molecule. This is in line with the covalent character of this system. Likewise, the charges on the C_2, C_3, and N_2 atoms

(23) Collard, K.; Hall, G. G. *Int. J. Quantum Chem.* **1977**, *12*, 623.

Table VIII. Calculated Bader and GAPT Atomic Charges in Trisubstituted Methanes and Their Conjugate Bases

system	atom	Q_{Bader} 6-31G*	Q_{GAPT} 6-31G*
CHF_3	H	0.0864	−0.0612
	C	2.1478	1.7895
	F	−0.7440	−0.5761
CF_3^-	C	1.3985	1.1823
	F	−0.7989	−0.7274
$CH(CN)_3$	H	0.1547	0.0663
	C	0.4156	0.6093
	C_{cyano}	1.2250	0.0244
	N	−1.4148	−0.2496
$C(CN)_3^-$	C	0.4029	−0.6500
	C_{cyano}	1.1527	0.6014
	N	−1.6205	−0.7180
$CH(NO_2)_3$	H	0.2045	0.0729
	C	1.0307	0.4987
	N	0.5424	1.2520
	O_1	−0.4690	−0.6970
	O_2	−0.4871	−0.7456
$C(NO_2)_3^-$	C	1.3379	−0.9195
	N	0.3595	1.6786
	O_1	−0.5694	−0.8527
	O_2	−0.5694	−0.8527

in the covalent minimum of the $C(NH_2)_3C(CN)_3$ species (**4**) parallel the charges in tricyanomethane, while the charges in the ionic minimum (**5**) parallel the charges in the tricyanomethanide anion. These trends are also evident in the covalent (**6**) and ionic (**7**) transition states of $C(NH_2)_3C(CN)_3$. A similar effect is present in the GAPT charges for the conformers of the $C(NH_2)_3C(NO_2)_3$ molecule. The GAPT charges on the C_2, N_2, O_1, and O_2 atoms are similar to the charges on the trinitromethanide anion, again indicating that this molecule is more an ion pair than a covalently bound system.

Conclusions

Ab initio electronic structure calculations provide a great deal of information on the electronic structures of hexasubstituted push–pull ethanes, revealing a spectrum of covalent and ionic bonding in these systems. Although such calculations are not feasible at present, inclusion of diffuse functions in the basis sets and accounting for the electron correlation effects may further stabilize the ionic isomers.

A plethora of molecules are known in which electron distributions are greatly influenced or even switched between two extreme cases by solvents or change of physical state. However, the fact that one molecule, namely, $C(NH_2)_3C(CN)_3$, exhibits two isomers stable in vacuo that have the same formal atomic connectivities, but entirely different electronic structures, is quite unusual in organic chemistry. Our studies have also shown that, depending on the substituent and conformation, the molecules can posses very complex topological structures. The bond paths in these topological structures not only exhibit unusual characteristics, but also can preclude accurate determination of Bader atomic charges due to the resulting complicated shapes of the zero-flux surfaces. The GAPT charge analysis, on the other hand, can help to clarify the interactions in these systems and to indicate the nature of the chemical bonds. We believe that these systems can serve as prototypes for understanding electron pushing and pulling

effects, or both inductive and mesomeric origin, in organic chemistry.

Acknowledgment. This work was partially supported by the National Science Foundation under the Contract CHE-9015566 and by the Florida State University through time granted on its VAX and Cray Y-MP digital computers. J.C. also acknowledges support from the Camille and Henry Dreyfus Foundation New Faculty Award Program. The helpful suggestions from Dr. J. P. Ritchie (Los Alamos National Laboratory, Theoretical Division, Group T-14) are appreciated.

Registry No. $(NH_2)_3CCF_3$, 134939-43-8; $(NH_2)_3CC(CN)_3$, 125041-94-3; $(NH_2)_3CC(NO_2)_3$, 125041-93-2.

Chemistry of Large Hydrated Anion Clusters $X^-(H_2O)_n$, $0 \leq n \approx 50$ and X = OH, O, O_2, and O_3. 1. Reaction of CO_2 and Possible Application in Understanding of Enzymatic Reaction Dynamics

X. Yang and A. W. Castleman Jr.*

Contribution from the Department of Chemistry, The Pennsylvania State University, University Park, Pennsylvania 16802. *Received February 4, 1991*

Abstract: The reactions of CO_2 with large hydrated anion clusters $X^-(H_2O)_{n=0-59}$, X = OH, O, O_2, and O_3, were studied in a fast-flow reactor under thermal conditions. Interesting solvation effects were found in terms of the observed mechanisms and reaction kinetics. Hydration by only a few water molecules makes O_2^- and O_3^- very inert to attack by CO_2 due to the change in sign of the reaction enthalpy from negative to positive caused by the solvation. In contrast, reactions of hydrated OH^- with CO_2 are exothermic at all degrees of solvation, and the large discrepancy between the experimentally measured rate constants and the theoretically calculated values, also attributable to solvation, can be explained by a consideration of the reaction kinetics in which the unimolecular dissociation rate constant of the reaction intermediate increases and the intermolecular conversion rate constant decreases at progressively larger cluster sizes. An application of this work is found in contributing to a further understanding of the reaction dynamics of enzymatic hydration of CO_2 in biological systems. The present work gives experimental evidence, by bridging the gas and the condensed phase via reactivity studies at different degrees of hydration, to support a proposed mechanism that attributes the enzymatic effect to a decrease in the hydration of OH^- by carbonic anhydrase.

Introduction

There are two prime motivations for studies of clusters: First, the research serves to bridge the gas and condensed phases since, as the degree of the solvation increases, the properties of large gas-phase clusters begin to approach those of the condensed phase.[1] Second, clusters are involved in many research fields like solvation, nucleation, aerosols, and fine particles and in processes such as combustion and catalysis. Investigations of clusters thus offer the promise of contributing to an understanding of these processes at the molecular level.[2] Large hydrated cluster ions are found to play an important role in many atmospheric processes.[3] However, most clusters have been produced and studied to date by using supersonic expansions and other nonthermal techniques,[4] which greatly limits the ability to investigate the properties and determine rates of reactions under well-defined temperatures and pressures. Several research groups have employed fast-flow techniques to study hydrated clusters under thermal conditions,[5] but due to past difficulties in producing large ones, only results with cluster sizes up to $n = 4$ have been reported in the literature for hydrated anionic species.[6]

Employing a flowing afterglow apparatus affixed with a high-pressure ion source, we demonstrated that clusters of $H^+(H_2O)_{n=1-60}$[7] and $X^-(H_2O)_{n=0-59}$ (X = OH, O, O_2, and O_3)[8] could be produced and investigated under well-defined temperatures and pressures. The selection of CO_2 as the reactant neutral in the present work is motivated by the extensive interest in its aqueous chemistry in terms of both environmental and biological sciences. Regarding the first area, there is recognized need for a continuing effort to identify reaction mechanisms of CO_2 that may influence its lifetime in the atmosphere and oceans. Similarly, although it is known that the enzymatic hydrolysis of CO_2 involves its reaction with OH^- in aqueous solution in the presence of enzymes as a catalyst, the basic reaction mechanism and dynamics of reaction of hydrated OH^- with CO_2 has yet to be fully elucidated.[9]

In previous studies, Fehsenfeld and Ferguson[10] determined the rate constants at room temperature for the reactions of CO_2 with various small hydrated anions $OH^-(H_2O)_{n=0-4}$, $O_2^-(H_2O)_{n=0-2}$, and $O_3^-(H_2O)_{n=0-2}$. In a later paper, Fehsenfeld et al.[11] reexa-

(1) Castleman, A. W., Jr.; Keesee, R. G. *Chem. Rev.* **1986**, *86*, 589. Castleman, A. W., Jr.; Keesee, R. G. *Acc. Chem. Res.* **1986**, *19*, 413.
(2) Castleman, A. W., Jr.; Keesee, R. G. *Science* **1988**, *241*, 36.
(3) Ferguson, E. E.; Fehsenfeld, F. C.; Albritton, D. L. In *Gas Phase Ion Chemistry*; Bowers, M. T., Ed.; Academic: New York, 1979; Vol. 1, p 45. Arnold, F. In *Atmospheric Chemistry*; Goldberg, E. D., Ed.; Springer-Verlag: Berlin, 1982; p 273. Keesee, R. G.; Castleman, A. W., Jr. *J. Geophys. Res.* **1985**, *90* (D), 5885.
(4) Märk, T. D.; Castleman, A. W., Jr. *Adv. At. Mol. Phys.* **1984**, *20*, 65.
(5) Meot-Ner, M.; Field, F. H. *J. Am. Chem. Soc.* **1977**, *99*, 998. Smith, D.; Adams, N. G.; Alge, E. *Planet. Space Sci.* **1981**, *29*, 449. Lau, Y. K.; Ikuta, S.; Kebarle, P. *J. Am. Chem. Soc.* **1982**, *104*, 1462. Viggiano, A. A.; Dale, F.; Paulson, J. F. *J. Chem. Phys.* **1988**, *88*, 2469. Zook, D. R.; Grimsrud, E. P. *J. Phys. Chem.* **1988**, *92*, 6374. Graul, S. T.; Brickhouse, M. D.; Squires, R. R. *J. Am. Chem. Soc.* **1990**, *112*, 631 and the references therein.
(6) Moruzzi, J. L.; Phelps, A. V. *J. Chem. Phys.* **1966**, *45*, 4617. Golub, S.; Steiner, B. *J. Chem. Phys.* **1968**, *49*, 5191. Ferguson, E. E. *Can. J. Chem.* **1969**, *47*, 1815. Arshadi, M.; Kebarle, P. *J. Phys. Chem.* **1970**, *74*, 1483. Melton, C. E. *J. Phys. Chem.* **1972**, *76*, 3116. Bohme, D. K. In *Ionic Processes in the Gas Phase*; Almoster Ferreira, M. A., Ed.; D. Reidel: Dordrecht, Holland, 1984; p 111. Hierl, P. M.; Ahrens, A. F.; Henchman, M.; Viggiano, A. A.; Paulson, J. F. *J. Am. Chem. Soc.* **1986**, *108*, 3140. Keesee, R. G.; Lee, N.; Castleman, A. W., Jr. *J. Am. Chem. Soc.* **1979**, *101*, 2599. Thompson, B. A.; Iribarne, J. W. *J. Chem. Phys.* **1979**, *71*, 4451 and references therein.
(7) Yang, X.; Castleman, A. W., Jr. *J. Am. Chem. Soc.* **1989**, *111*, 6845.
(8) Yang, X.; Castleman, A. W., Jr. *J. Phys. Chem.* **1990**, *94*, 8500.
(9) For example, *Catalytic Activation of Carbonic Dioxide*; Ayers, W. M., Ed.; ACS Symposium Series 363; American Chemical Society: Washington, DC, 1988. *Enzymatic and Model Carboxylation and Reduction Reactions for Carbon Dioxide Utilization*; Aresta, M., Schloss, J. V., Eds.; Kluwer Academic Publishers: Boston, 1990.
(10) Fehsenfeld, F. C.; Fergusson, E. E. *J. Chem. Phys.* **1974**, *61*, 3181.

0002-7863/91/1513-6766$02.50/0